Nuclear Instruments and Methods in Physics Research A 658 (2011) 90–97

Contents lists available at ScienceDirect

Nuclear Instruments and Methods in Physics Research A

journal homepage: www.elsevier.com/locate/nima

New BNL 3D-Trench electrode Si detectors for radiation hard detectors for sLHC and for X-ray applications

Zheng Li *

Brookhaven National Laboratory, NY 11973-5000, USA

ARTICLE INFO

Available online 11 May 2011

Keywords:
3D electrode Si detectors
Radiation
Damage
Hardness
3D-Trench electrode detectors
Independent Coaxial Detector Array (ICDA)
3D-Trench-CJ
3D-Trench-ORJ

ABSTRACT

A new international-patent-pending (PCT/US2010/52887) detector type, named here as 3D-Trench electrode Si detectors, is proposed in this work. In this new 3D electrode configuration, one or both types of electrodes are etched as trenches deep into the Si (fully penetrating with SOI or supporting wafer, or non-fully penetrating into 50–90% of the thickness), instead of columns as in the conventional ("standard") 3D electrode Si detectors. With trench etched electrodes, the electric field in the new 3D electrode detectors are well defined without low or zero field regions. Except near both surfaces of the detector, the electric field in the concentric type 3D-Trench electrode Si detectors is nearly radial with little or no angular dependence in the circular and hexangular (concentric-type) pixel cell geometries. In the case of parallel plate 3D trench pixels, the field is nearly linear (like the planar 2D electrode detectors), with simple and well-defined boundary conditions. Since each pixel cell in a 3D-Trench electrode detector is isolated from others by highly doped trenches, it is an electrically independent cell. Therefore, an alternative name "Independent Coaxial Detector Array", or ICDA, is assigned to an array of 3D-Trench electrode detectors. The electric field in the detector can be reduced by a factor of nearly 10 with an optimal 3D-Trench configuration where the junction is on the surrounding trench side. The full depletion voltage in this optimal configuration can be up to 7 times less than that of a conventional 3D detector, and even a factor of two less than that of a 2D planar detector with a thickness the same as the electrode spacing in the 3D-Trench electrode detector. In the case of non-fully penetrating trench electrodes, the processing is true one-sided with backside being unprocessed. The charge loss due to the dead space associated with the trenches is insignificant as compared to that due to radiation-induced trapping in sLHC environment. Since the large electrode spacing (up to 500 μm) can be realized in the 3D-Trench electrode detector due to their advantage of greatly reduced full depletion voltage, detectors with large pixel cells (therefore small dead volume) can be made for applications in photon science (e.g. X-ray).

1. Introduction

For Si detector applications at the LHC (Large Hadron Collider) upgrade, the Super-LHC (sLHC), the expected radiation level for the inner-most detectors will be 10 times higher than that in the current LHC, up to 1×10^{16} n_{eq}/cm^2. In this case, in addition to the detector full depletion problem, the trapping problem is now one of the main limiting factors to the detector CCE (charge collection efficiency).

Developed by Parker at University of Hawaii [1,2], the conventional 3D electrode detector is named for the way it is processed. Different from planar technology, p+ and n+ electrodes in columns with a typical diameter of 10 μm are etched and doped along the detector thickness ("3D" processing), as shown in Fig. 1. The depletion develops laterally between the p^+ and n^+ electrodes, whose spacing is defined here as λ_C (column spacing or electrode spacing). The detector full depletion voltage thus just depends on the p^+–n^+ separation λ_C, and it is insensitive to detector thickness. Since this separation can be made very small (<100 μm), much lower voltage will be needed to fully deplete the detector, thereby providing much higher radiation tolerance at much lower biases. In addition, the column spacing λ_C can be made on the order of 30–50 μm, close to the trapping distance of free carriers in Si after radiation of high fluences (near 1×10^{16} n_{eq}/cm^2) [3], so that the carrier trapping can also be greatly reduced, thus improving the detector charge collection. Although there have been a number of variants of the conventional 3D electrode detectors in recent years, namely the single-type-column (3D-STC) [4,5], one-sided 3D [5–7], and double-sided 3D [8–10], the electrodes are still in the shape of

* Tel.: +1 631 344 7604; fax: +1 631 344 5773.
E-mail address: zhengl@bnl.gov

0168-9002/$ - see front matter © 2011 Elsevier B.V. All rights reserved.
doi:10.1016/j.nima.2011.05.003

column. There was a trench-wall-electrode proposed by Kenney et al. [11], where the detector boundary was etched and doped as trench-wall for the fabrication of edgeless or active-edge detectors, while the electrodes in the bulk are column ones. The electric field profiles in these detectors with column electrodes are very non-homogeneous; there are saddle points in the electric potential where regions of low or zero electric field exist. Also,very high electric fields exist near the junction column [6]. These non-homogeneous electric field profiles can cause (1) intrinsic breakdown near the junction column, especially after heavy irradiation; (2) long carrier transient time duo to initial diffusion in the low field region, causing incomplete charge collection; (3) much large depletion voltage (as compared to a planar 2D detector with a thickness the same as the column spacing) especially after irradiation.

In order to avoid confusion in names with other 3D technologies and detectors, namely 3D stacking of detectors and electronics and 3D position-sensitive detectors, we will now call the 3D Si detectors as "3D electrode" Si detectors. The conventional 3D electrode detectors described in [1,2,4–10] and shown in Fig. 1 will be thus called standard 3D electrode Si detectors.

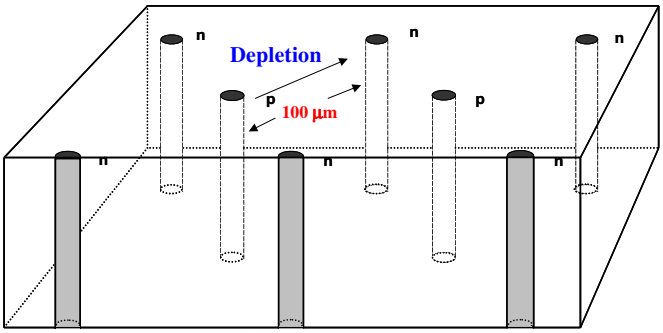

Fig. 1. Illustration of a conventional 3D electrode Si detector: electrodes are cylindrical columns etched into Si [2].

In this paper, we propose a new electrode configuration, called "Trench", and a new type of 3D electrode detectors: 3D-Trench electrode detectors. Since in these types of 3D-trench electrode detectors, the central electrode is surrounded by a trench electrode (e.g. Fig. 2), each cell is therefore electrically isolated from other cells. We therefore give it an alternative name as "Independent Coaxial Detector Array" (ICDA). BNL has filed US and International patent applications [12,13] for the "3D Trench Electrode Detector and Independent Coaxial Detector tor Array" as described in this paper and the initial concept has been described in [14]. The isolation of cells from each other in an ICDA may be advantageous for x-ray detector applications; this is discussed later.

2. Concept and electric field calculations of the new 3D-trench electrode detectors

2.1. Various 3D-trench configurations

As shown in Fig. 2a for a single-cell of the new 3D-Trench electrode detector with hexangular shape, both the trench and center column electrodes are etched and doped deep into the Si bulk. Similar to the previous BNL's one-sided 3D electrode detectors [5,6], the electrodes do not penetrate the bottoms silicon surface. While for thin wafers, $d \leq 300$ μm, an un-etched thickness of as small as $l = d - 20$ μm may be possible with good control; for larger wafer thicknesses, the value of l may be larger than $d - 20$ μm, and its precision may largely depend on the type of deep reactive ion etch (DRIE) technology. In a single cell, the electric field is mostly homogeneous (almost no θ and z dependence in a cylindrical coordinates, e.g. Fig. 4), except near both surfaces. An array of a single cell can form a detector with each cell nearly electrically independent of each other, namely the "Independent Coaxial Detector Array" (ICDA). As shown in Fig. 2b, for all types of our ICDA discussed in the paper, the signal will be

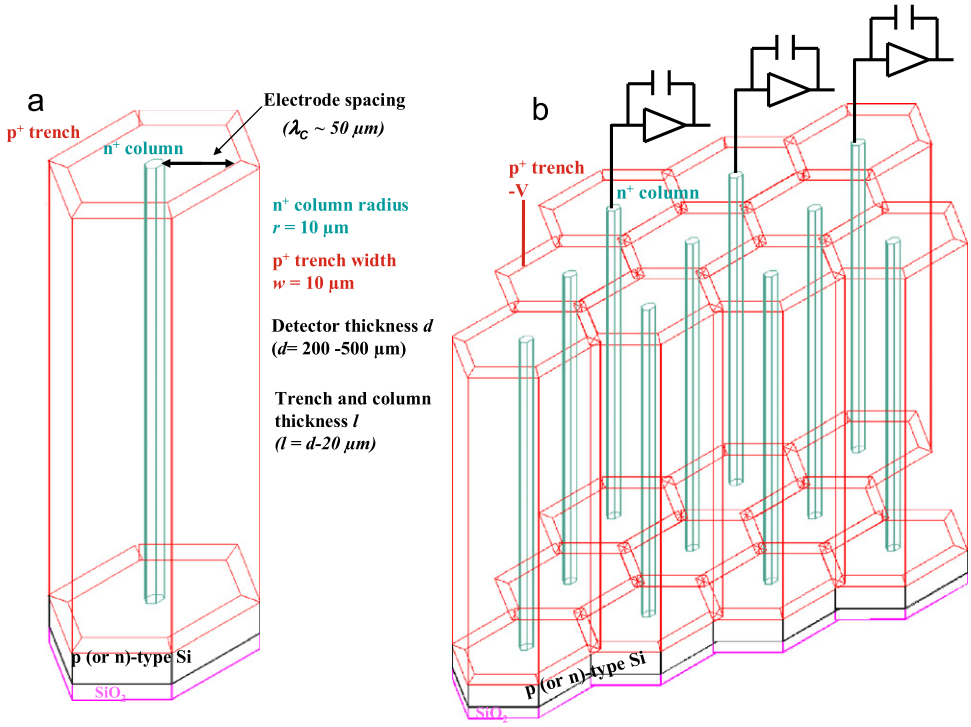

Fig. 2. A single cell of the new 3D-Trench electrode Si detector (hexangular type) (a), and an array of cells to form a detector (ICDA) (b).

read from the central electrodes with much reduced capacitance (for pixel detectors in particular).

Fig. 3 shows various common configurations of a single ICDA cell with concentric central column or short central trench electrodes, and parallel plate type with long central trench electrodes. There can be numerous other geometries which are not illustrated here.

2.2. One dimensional simulations of concentric 3D-Trench electrode detectors

2.2.1. 3D-Trench electrode detectors with central junction column (3D-Trench-CJ)

For more uniform electric field distribution in the detector, a cylindrical unit cell is preferred; it requires a small cylindrical column central electrode (diameter about 10 μm) and a cylindrical trench (about 10 μm in width) outer electrode. For the most efficient packing in space, however, a hexangular unit cell as shown in Fig. 2 is preferred. Since in our 3D-Trench Electrode detectors, there is an asymmetry in electrodes, we can have two different types of detectors for the same single cell geometry: (1) the junction is at the center electrode column (3D-Trench-CJ); and (2) the junction is at the outer ring trench (3D-Trench-ORJ). The electric field in a hexangular unit cell can be approximated by that for a cylindrical one. Shown in Fig. 4 are cylindrical geometries

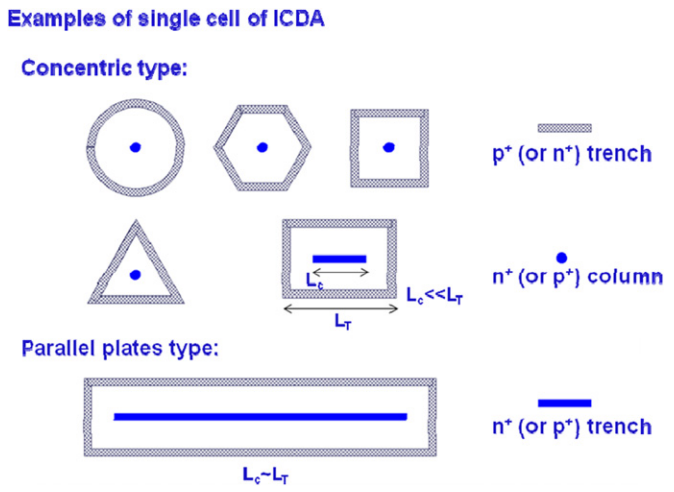

Fig. 3. Some common configurations of a single cell of 3D-Trench electrode detectors.

(r, θ, z) and boundary conditions for 3D-Trench-CJ and 3D-Trench-ORJ types. Here w_n and w_p are the absolute distances measured from the point of $r=r_C$, the radius of the central column. The radius of the outer ring trench is R. Here we use p-type bulk as an example for radiation-hard detector. Both n-type and p-type bulk can be used and the junction location will change accordingly.

Analytical calculations of electric potential and field profiles in a single cell of a 3D-trench-CJ Si detector can be obtained using a cylindrical geometry. The electric field is mostly homogeneous (no θ and z dependence) within the cell, with only r dependence, except in the regions near the two ends of the central column.

By solving the Poisson equations

$$\begin{cases} \frac{1}{r}\frac{d}{dr}(rE(r)) = \frac{eN_d}{\varepsilon\varepsilon_0} & (r_C - w_n \le r < r_C) \\ \frac{1}{r}\frac{d}{dr}(rE(r)) = -\frac{eN_{eff}}{\varepsilon\varepsilon_0} & (r_C \le r \le w_p) \end{cases} \quad (1)$$

with boundary conditions

$$\begin{cases} E(r_C - w_n) = 0 \\ E((r_C)^-) = E((r_C)^+) \\ E(w_P) = 0 \end{cases} \quad (2)$$

We can get the electric field in a single cell

$$E(r) = \begin{cases} 0 & (r < r_C - w_n) \\ \frac{1}{2}\frac{eN_d}{\varepsilon\varepsilon_0} r\left[1 - \frac{(r_C - w_n)^2}{r^2}\right] & (r_C - w_n \le r < r_C) \\ \frac{1}{2}\frac{eN_{eff}}{\varepsilon\varepsilon_0} r\left[\frac{(r_C + w_p)^2}{r^2} - 1\right] & (r_C \le r < r_C + w_p) \\ 0 & (r \ge r_C + w_p) \end{cases} \quad (3)$$

where N_d, r_C, and w_n are the doping concentration, the radius, and depletion depth of the n^+ column, respectively; N_{eff} and w_p are effective doping concentration and depletion depth in the p-type bulk, respectively.

For most cases, $N_{eff}/N_d < 10^{-5}$ even after irradiation to 1×10^{16} n_{eq}/cm^2, w_n is much smaller than w_p ($w_n/w_p < 10^{-4}$) and r_C ($w_n/r_C < 10^{-3}$). Carrying out the integration $\int_{r_C - w_n}^{r_C + w_p} E(r)\ dr = V + V_{bi}$ gives the simplified equation to solve w_p:

$$(r_C + w_p)^2 \ln\frac{r_C + w_p}{r_C} - \frac{1}{2}\left[(r_C + w_p)^2 - r_C^2\right] = \frac{2\varepsilon\varepsilon_0(V + V_{bi})}{eN_{eff}} \quad (4)$$

where V is the absolute value of the applied reverse voltage and V_{bi} is the build-in potential. The electric field in the p-type bulk can be calculated with

$$E(r) = \frac{1}{2}\frac{eN_{eff}}{\varepsilon\varepsilon_0} r\left[\frac{(r_C + w_p)^2}{r^2} - 1\right] \quad (r_C \le r < r_C + w_p) \quad (5)$$

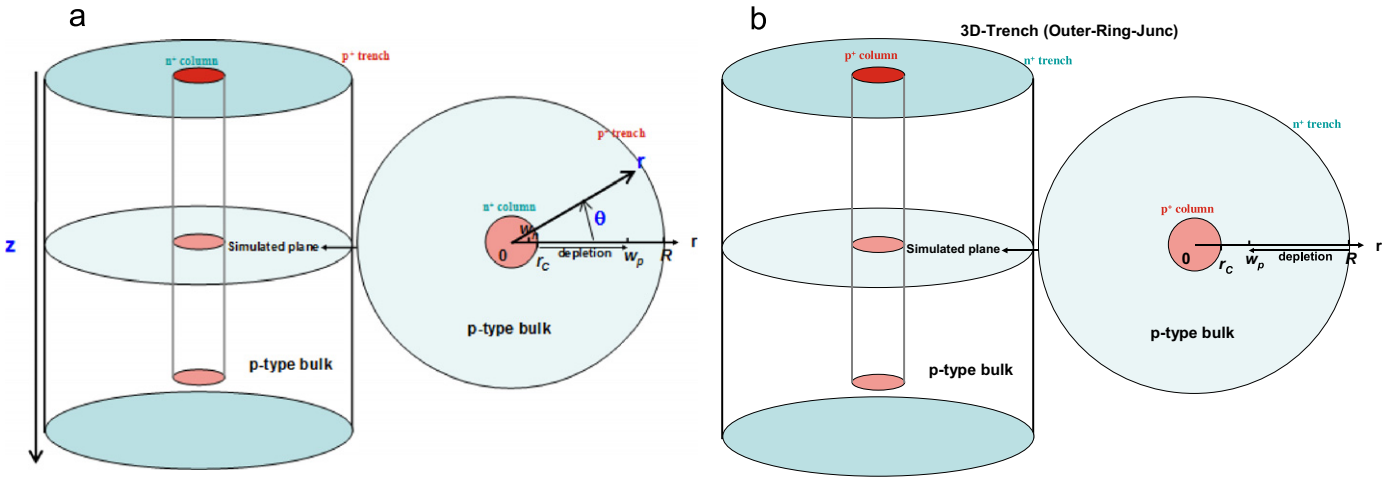

Fig. 4. Illustrations of a cylindrical geometry for the electric field calculation of 3D-Trench Si detectors: (a) 3D-Trench-CJ and (b) 3D-Trench-ORJ.

In the case of over depletion, we have

$$E(r)=\frac{1}{2}\frac{eN_{\rm eff}}{\varepsilon\varepsilon_0}r\left[\frac{R^2}{r^2}-1\right]+\frac{V-V_{\rm fd}}{r\ln R/r_{\rm C}}$$
$$(r_{\rm C}\le r\le R)\quad(\text{for 3}D\text{-Trench-CJ}) \tag{6}$$

where the full depletion voltage $V_{\rm fd}$ can be solved by the following equation:

$$V_{\rm fd}=\frac{eN_{\rm eff}}{2\varepsilon\varepsilon_0}\left[R^2\ln\frac{R}{r_{\rm C}}-\frac{1}{2}(R^2-r_{\rm C}^2)\right]-V_{\rm bi}\quad(\text{for 3}D\text{-Trench-CJ}) \tag{7}$$

As the detector is irradiated by neutrons and charged particles, the effective doping concentration $N_{\rm eff}$ will increase linearly with 1 MeV neutron-equivalent fluence $\Phi_{\rm neq}$ at high fluences

$$N_{\rm eff}\approx b\Phi_{\rm neq}\quad(\text{for }\Phi_{\rm neq}>10^{14}\,{\rm n_{eq}/cm^2}) \tag{8}$$

The proportional constant is about 0.01 $\rm cm^{-1}$ for oxygenated Si detectors irradiated with high energy protons and 0.02 for neutron irradiations [15]. As can be seen in Eq. (7), the detector full depletion voltage is proportional to $N_{\rm eff}$.

As can be seen in Fig. 5a, a non-irradiated 3D-Trench-CJ electrode detector with $R=40\,\mu$m and $N_{\rm eff}=1\times10^{12}\,\rm cm^{-3}$ can be fully depleted at a bias voltage of 2.03 V and the electric field is highly concentrated near the central junction column, at a value of about 2600 V/cm. For an irradiated ($1\times10^{16}\,\rm n_{eq}/cm^2$) 3D-Trench-CJ electrode detector with the same geometry and $N_{\rm eff}=1\times10^{14}\,\rm cm^{-3}$, however, the full depletion voltage and highest electric field are 100 times higher, at 206 volts and 2.6×10^5 V/cm, respectively. The factor of 100 is in fact that of the ratio of $N_{\rm eff}$. Also plotted in Fig. 5b is the electric field profile of an irradiated ($1\times10^{16}\,\rm n_{eq}/cm^2$) planar 2D Si detector with a thickness the same as that of the electrode spacing in our 3D-Trench-CJ electrode detector (i.e. $d_{\rm 2D}=R-r_{\rm C}$). At 206 V bias voltage, the planar 2D Si detector is already much over-depleted, indicating a much smaller full depletion voltage than that of a 3D-Trench-CJ electrode detector. In fact, $V_{\rm fd}(2{\rm D})=eN_{\rm eff}d_{\rm 2D}^2/2\varepsilon\varepsilon_0-V_{\rm bi}$, using Eq. (7), we have (for. $d_{\rm 2D}=R-r_{\rm C}$)

$$\frac{V_{\rm fd}(3D\text{-Trench-CJ})}{V_{\rm fd}(2{\rm D})}\cong\frac{[R^2\ln R/r_{\rm C}-(1/2(R^2-r_{\rm C}^2))]}{(R-r_{\rm C})^2}$$
$$\cong\ln\frac{R}{r_{\rm C}}-\frac{1}{2}\quad(\text{for }R\gg r_{\rm C}) \tag{9}$$

So this ratio is in the order of $\ln(R/r_{\rm C})$, and is about 2 for our case of $R=40\,\mu$m and $r_{\rm C}=5\,\mu$m, and will increase with $R/r_{\rm C}$, although slowly. We note here that the thickness of the 3D-trench electrode detector is not specified, and it can be much bigger than that of the 2D detector (here at 35 μm), say $d=300\,\mu$m. Therefore the full depletion voltage can still be much smaller than that of a 2D detector with the same thickness. In fact the ratio is $R^2\ln(R/r_c)/d^2$.

2.2.2. 3D-Trench electrode detectors with outer trench ring as the junction (3D-Trench-ORJ)

As we have seen that, due to the small junction electrode effect, the electric field is concentrated near the central $\rm n^+$ electrode in a 3D-Trench-CJ electrode Si detector with p-type bulk. Although the electric field is almost homogeneous along the θ and z coordinates with only r dependence, high electric field near the central electrode column can cause breakdown and much higher depletion voltage than the standard 2D planar detector with $d_{\rm 2D}=R-r_{\rm C}$ (Eq. (9)). This will make large electrode spacing ($R>250\,\mu$m) not practical in 3D-Trench-CJ electrode (and also in standard 3D electrode) Si detectors. Much better electric field can be achieved in a 3D-trench detector if the junction (high electric field) is at the outer ring of trench, as shown in Fig. 6. In this case, the $\rm n^+/p$ junction is formed by the outer ring trench that was made $\rm n^+$. The central collecting electrode column is now made $\rm p^+$ and it is the Ohmic contact with low field. We now define this type of 3D-Trench detector as the 3D-Trench-ORJ (outer-ring-junction). We note here that for n-type bulk, one

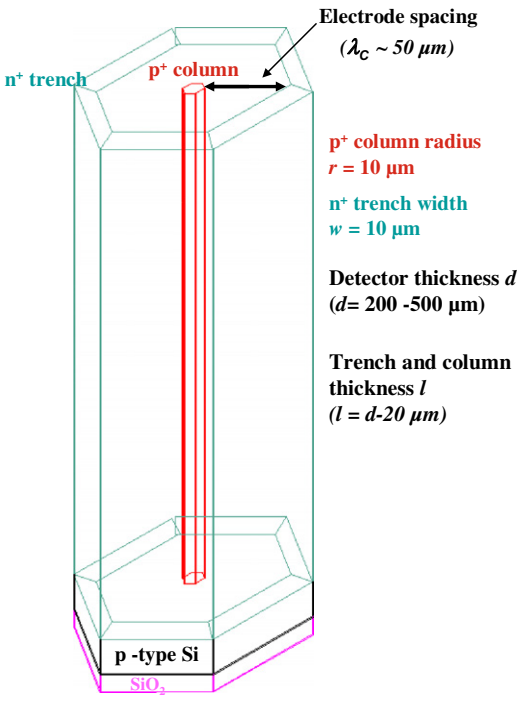

Fig. 6. A single cell of the new 3D-Trench electrode Si detector (hexangular type) with outer-ring-junction (3D-Trench-ORJ) on p-type substrate.

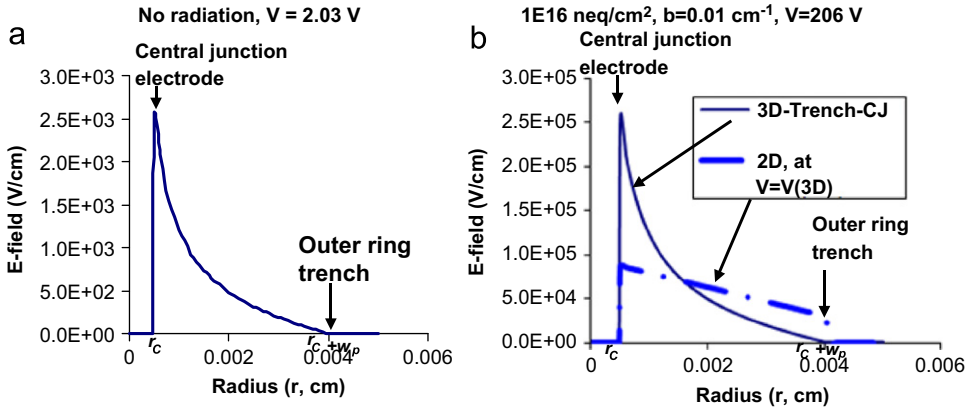

Fig. 5. Electric field profile in a single cell of a non-irradiated (a) and irradiated 3D-Trench-CJ electrode detectors.

needs to simply make the switch of $n^+ \leftrightarrow p^+$, $p \leftrightarrow n$, and $e \leftrightarrow h$ in all of our calculations and figures below.

Similarly, one can calculate the electric field in the bulk as before using the geometry and boundary condition shown in Fig. 4b:

$$E(r) = -\frac{eN_{\text{eff}}}{2\varepsilon\varepsilon_0} r\left[1-\frac{(R-w_p)^2}{r^2}\right] \quad (r_C < R-w_p \le r \le R) \tag{10}$$

and w_p is determined by:

$$\frac{1}{2}\left[R^2-(R-w_p)^2\right]-(R-w_p)^2\ln\frac{R}{R-w_p} = \frac{2\varepsilon\varepsilon_0(V+V_{\text{bi}})}{eN_{\text{eff}}} \tag{11}$$

At the condition of over-depletion, the electric field profile in a 3D-Trench-ORJ can be found as

$$E(r) = -\frac{1}{2}\frac{eN_{\text{eff}}}{\varepsilon\varepsilon_0} r\left[1-\frac{r_C^2}{r^2}\right]-\frac{V-V_{\text{fd}}}{r\ln R/r_C} \quad (r_C \le r \le R) \quad (\text{for } 3D\text{-Trench-ORJ}) \tag{12}$$

where the full depletion voltage is

$$V_{\text{fd}} = \frac{eN_{\text{eff}}}{2\varepsilon\varepsilon_0}\left[\frac{1}{2}(R^2-r_C^2)-r_C^2\ln\frac{R}{r_C}\right]-V_{\text{bi}} \quad (\text{for } 3D\text{-Trench-ORJ}) \tag{13}$$

The electric field of a 3D-Trench-ORJ Si detector, irradiated to 1×10^{16} n_{eq}/cm^2, is plotted in Fig. 7, along with that of a 2D planar Si detector with $d_{2D}=R-r_C$ at a bias of 69 V, 10 V over the full depletion voltage of the 3D-Trench-ORJ Si detector. The differences in electric field in a 3D-Trench-ORJ are striking: (1) the electric field profile is nearly linear, in fact it is slightly sub-linear; (2) its full depletion voltage is about one half of that of the planar 2D detector, and less than 1/3 times of that of the 3D-Trench-CJ (Fig. 5); (3) the maximum electric field is near the outer ring trench, and it is about 30% less than that of the 2D planar detector and is about 1/9 of that of the 3D-Trench-CJ (Fig. 5); and (4) at over-depletion, the extra field mostly increases at the originally low-field region near the central column with very little increase at outer ring trench. These comparisons between 2D planar, 3D-Trench-CJ and 3D-Trench-ORJ detectors are summarized in Table 1. It is clear that even at the highest radiation fluence (1×10^{16} n_{eq}/cm^2), the 3D-Trench-ORJ Si detectors can be operated at full depletion with maximum electric field much below the breakdown field of 3×10^5 V/cm in Si. While for the 3D-Trench-CJ (and so for the standard 3D electrode) detectors, the maximum electric field can be dangerously close to the breakdown field.

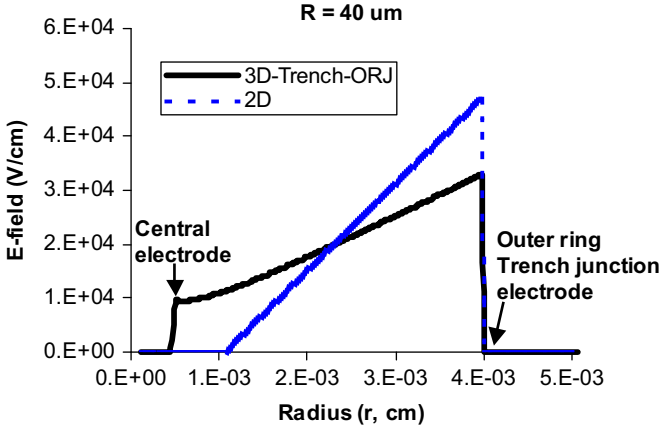

Fig. 7. Comparisons of electric field profiles (absolute values plotted here, E-fields are negative) in a 3D-Trench-ORJ electrode detector (at over-depletion) and in a 2D planar detector.

Again we can obtain the full depletion ratio, we have (for $d_{2D}=R-r_C$)

$$\frac{V_{\text{fd}}(3D\text{-Trench-ORJ})}{V_{\text{fd}}(2D)} \cong \frac{[1/2(R^2-r_C^2)-r_C^2\ln R/r_C]}{(R-r_C)^2} \cong \frac{1}{2} \quad (\text{for } R \gg r_C) \tag{14}$$

Again the discussion about ration of full depletion voltages of 3D-trench electrode and 2D detectors apply here. The ration here now is about $1/2(R^2/d^2)$. The calculation of the weighting potential and field is quite simple as well for the cylindrical geometry and we have

$$\begin{cases} \Phi_w(r) = \frac{\ln(r/R)}{\ln(r_C/R)} \\ E_w(r) = \frac{1}{r}\frac{1}{\ln(R/r_C)} \end{cases} \tag{15}$$

The induced current [16,17] and charge (collected charge) by a MIP (minimum ionizing particle) can also be obtained, though numerically. Due to the length limitation of the paper, only the results are presented here as shown in Fig. 8 for an irradiated (1×10^{16} n_{eq}/cm^2) 3D-Trench-ORJ with the trapping time constant obtained in Refs. [18–22].

As shown in Fig. 8a, the current transients are very fast at a modest bias voltage of 96 V, less than 0.4 ns. Fig. 8b shows that the total collected charge will also change with particle incident position in a 3D-Trench-ORJ electrode detector. This is due to the fact that the probability of hole trapping and electron trapping will change with the particle incident position, which in turn, together with the weighting field profile, will affect the composition of electron and hole contributions and therefore the total collected charge. This position dependence of total collected charge is true also for 3D-Trench-CJ electrode detectors and for standard 3D electrode detectors with column electrodes.

2.3. Dead space considerations

The main disadvantage of the 3D-Trench electrode detector is the dead space in detector sensitive volume due to the trench etching. The trenches will act as voids in the detector bulk, thus causing the fill factor degradation in the detector. However, as we simulated below, for different applications this reduction in sensitive volume may not cause significant problem in the applications of 3D-Trench electrode Si detector.

For sLHC applications with extreme irradiation fluence and large trapping, R should be made small. For the smallest possible R of 40 μm, the dead space is about 16% as shown in Fig. 9. But as we have seen before, the charge collection efficiency in a 3D-Trench electrode Si detector can be as high as 50% at 1×10^{16}

Table 1
Comparisons of detector characteristics among 2D planar, 3D-Trench-CJ, and 3D-Trench-ORJ Si detectors at 1×10^{16} n_{eq}/cm^2.

	Full depletion voltage of 35 μm (V)	Maximum electric field located at/value (at $V=V_{fd}$)	Form of electric field	Depletion depth at 59V (μm)
2D planar/3D-trench (rectangular type)	99	Junction electrode/5.7×10^4 V/cm (99 V)	Linear	27
3D-Trench-CJ	206	Central electrode column/2.55×10^5 V/cm (206 V)	Super-linear	21
3D-Trench-ORJ	59	Outer-ring trench/3.19×10^4 V/cm (59 V)	Slightly sub-linear	35

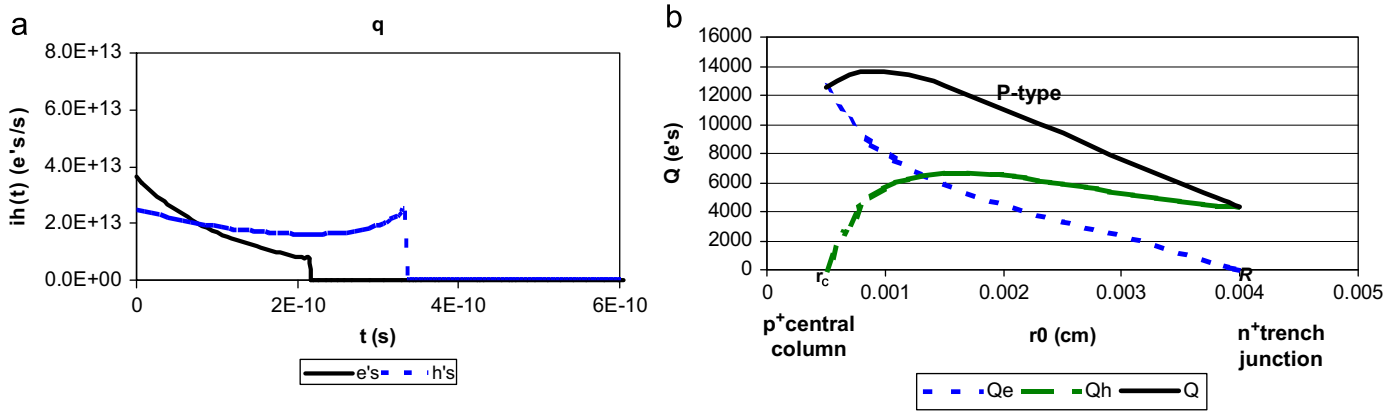

Fig. 8. Electron and hole induced currents (a) by a MIP in an irradiated (1×10^{16} n_{eq}/cm^2) 3D-Trench-ORJ electrode Si detector. MIP incident point is at the middle point between the central junction column (r_C=5 μm) and the outer ring (R=40 μm), d_{eff}=290 μm, V=96 V (V_{fd}=59 V), $E_{max}=1.59\times10^5$ V/cm; and induced charges as a function of MIP incident position (b) (average is about 50%).

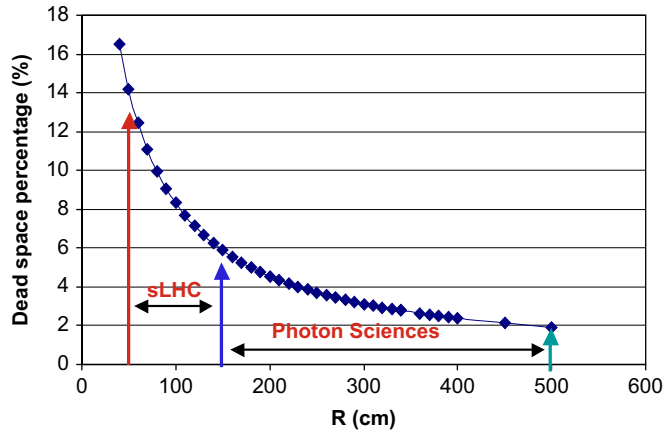

Fig. 9. Percentage of dead space in 3D-Trench (hexangular type) electrode Si detectors. r_C=5 μm, and trench width w=10 μm.

n_{eq}/cm^2 irradiation. The 16% dead space will reduce the overall CCE to about 42%, which is still much higher than that of a 2D planar Si detector at about 10%.

For the application in X-ray detection and energy spectroscopy, there is no trapping and R can be made large, from 100 to 500 μm. At R=100 μm, the dead space is about 8%, and at R=500 μm, it is less than 2%! In current multi-element (pixel) X-ray detectors, a metal grid has to be used to block the X-ray from entering the boundary regions between the neighboring pixels to isolate pixels from each other. The width of the grid can be larger than 100 μm, creating a dead space much larger than that due to the trenches.

3. 3D-Trench electrode Si detectors for X-ray applications

As we have stated above, the 3D-Trench-ORJ configuration is the best due to its near homogeneous electric field distribution; and much lower electric field and full depletion voltage than other 3D electrode configurations and even the conventional planar 2D detectors. These advantages provide good basis for X-ray applications in photon science. A usual aspect of X-ray applications is that there is little or no displacement damage (or bulk damage) that can cause free carrier trapping,; this greatly relaxes the requirement of the electrode spacing compared to sLHC applications. In fact, due the much smaller depletion voltage need for 3D-Trench-ORJ electrode Si detectors, one can easily make electrode spacing as large as 500 μm, which can make the pixel pitch as large as 1 mm. Furthermore, one can make the

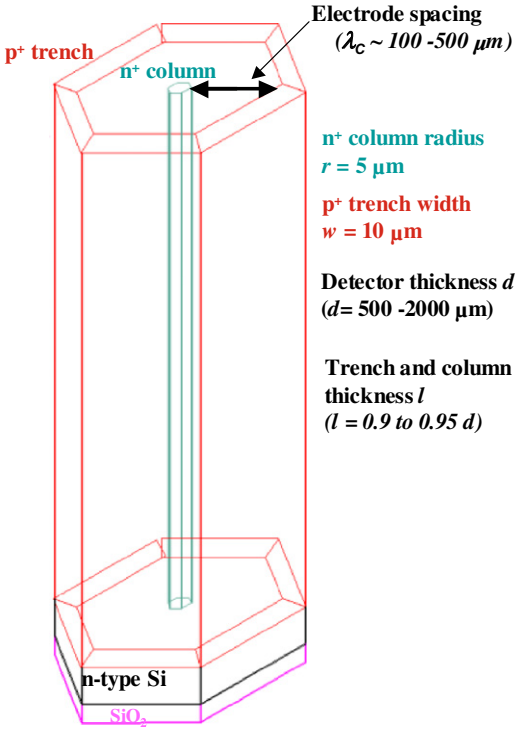

Fig. 10. A single cell of the new 3D-Trench-ORJ electrode Si detector on n-type substrate.

detector thickness as large as 1–2 mm for high detection efficiencies into 10's of keV hard X-ray, depending on the deep reactive ion etching (DRIE) technology and requirement on the aspect ratio of the etching depth to the etching width, which can be made 25–30 to 1, with the hope of higher aspect ratio in future DRIE technology. As the electrode spacing increases (or R increases), the percentage of dead space due to the trenches will be greatly reduced, to less than 2%. In addition, since all pixels are isolated from each other due to the separation by trench walls, the tail in energy spectrum can be greatly reduced, thus improving the peak to valley ratio and the energy resolution.

Shown in Fig. 10 is a single cell of a 3D-Trench-ORJ electrode Si detector for X-ray applications. The bulk is chosen as n-type for easy processing. The electrode spacing can be from 10's of μm to 100's of μm, depending on the application needs. For typical applications, it can be 100–500 μm, which will give pixel pitches from 200 μm to 1 mm.

In order to isolate the central collecting n^+ columns, a p^+ spray ion implantation is needed on the backside before the full detector processing. Since no photolithography is needed for this step and no further processing are performed on the backside, the detector processing is still a one-sided one. As can be seen also in the figure, the area of collecting electrode can be very small ($\sim$100 μm^2), and the capacitance of each pixel is dominated by the length of the n^+ column, which can be less than 0.2 cm (maximum length) $\times$ 0.5 pF/cm = 0.1 pF. Small capacitance can in turn ensure small noise, thus improving the detector's X-ray energy resolution (similar to the Si drift detector (SDD), but with much smaller bias voltages).

4. 3D simulation results

Full 3D simulations have also been performed with full boundary conditions on both surfaces with oxide charges, for various geometries. Again due to paper length limitation, we will only show a few results on the square/rectangular geometries.

Fig. 11 shows the 3D simulation results of electric field and hole concentration of a p-type 3D-Trench-ORJ with square geometry after irradiation to 1×10^{16} n_{eq}/cm^2. The single square cell simulated here has a size of 130 $\mu m \times 130$ μm in area, including the n^+ trench with a width of 10 μm that surrounds the center p^+ collection column that has an area of 10 $\mu m \times 10$ μm. The wafer thickness is 300 μm, and it is p-type with an effective doping density of $1 \times 10^{14}/cm^2$. The depth for both the trench and column here is 270 μm. It is clear that at a bias voltage of 240 V, the whole detector is depleted, including the volume where the trench and column are not penetrating. The 240 V full depletion voltage is even less than that of a 2D planar detector with a thickness the same as that of the electrode spacing here (50 μm).

Fig. 12 shows the 3D simulation results of hole concentration of a p-type 3D-Trench-ORJ of the parallel plate type with rectangular geometry after irradiation to 1×10^{16} n_{eq}/cm^2. The single cell of the parallel plate type with rectangular geometry simulated here has a size of 130 $\mu m \times 280$ μm in area, including the n^+ trench with a width of 10 μm that surrounds the center p^+ collection trench that has an area of 10 $\mu m \times 160$ μm. The wafer thickness is 300 μm, and it is p-type with an effective doping density of $1 \times 10^{14}/cm^2$. The depth for both types of trenches here is 270 μm. At a bias voltage of 240 V, while the volumes at the two ends of the central trench plane (Fig. 12a, concentric geometry) are fully depleted, the volumes along the central trench plane (Fig. 12b, parallel-plate (2D) geometry) are still not fully depleted, confirming again our finding just stated above—i.e. the full depletion voltage of a 3D-Trench-ORJ detector of the concentric geometry is less than that of a 2D planar detector with a thickness the same as that of the electrode spacing here (50 μm).

5. Discussions and conclusion

As we demonstrated in the paper, while some features of the new BNL 3D-Trench-CJ detectors are the same as those of the standard 3D electrode detectors with column electrodes (such as high electric field at the junction column, and higher full depletion voltage as compared to 2D planar detector with a thickness the same as the electrode spacing), the electric field in a concentric

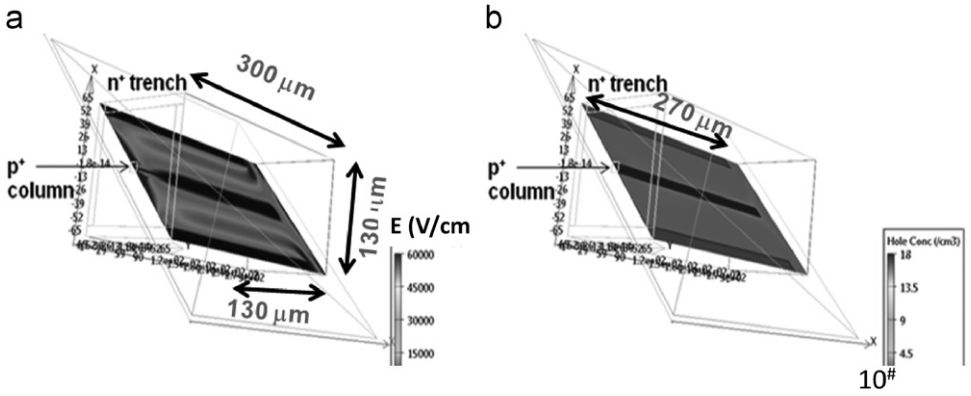

Fig.11. 3D simulations of (a) electric field and (b) hole concentrations of an irradiated p-type 3D-Trench-ORJ detector with square geometry. Width of the n^+ trench and p^+ column is 10 μm.

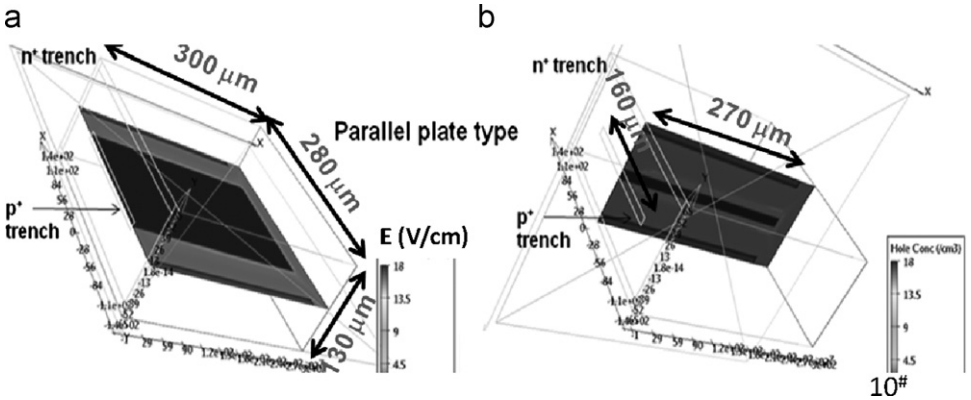

Fig.12. 3D simulations of hole concentration of an irradiated p-type 3D-Trench-ORJ detector of the parallel plate type with rectangular geometry: (a) a cut plane along the central trench and (b) a cut plane perpendicular (at the middle of) to the central trench. Width of the n^+ and p^+ trench is 10 μm.

type (e.g. near circular such as hexangular geometry) 3D-Trench-CJ detector is much more homogeneous with nearly only radial dependence. There are no potential saddle points and no low field regions in the middle of the detector as is the case for standard 3D electrode detectors. The best configuration for the new BNL 3D-Trench-electrode detector is the one with junction on the outer ring trench with a small central column of the ohmic type as the collection electrode, or the 3D-Trench-ORJ. The 3D-Trench-ORJ Si detectors with small pitches ($<100\ \mu m$) can be used for sLHC applications for greatly improved radiation hardness, and those with large pitches ($100\ \mu m < P < 1000\ \mu m$) can be used for applications in photon science. The advantages of 3D-Trench-ORJ Si detectors are: (1) electric filed profile in the detector can be nearly uniform; (2) much smaller maximum electric field than those in 3D-Trench-CJ and standard 3D electrode Si detectors; even smaller than that in the 2D planar Si detectors with a thickness the same as that of the electrode spacing. For X-ray applications with minimum displacement damage, (3) the detector thickness can be as large as 2 mm for better detection efficiencies to hard X-ray; (4) the pixel pitch can be made as large as 1 mm without risking large bias voltage due to much lower full depletion voltage as compared to other detector structures; (5) small capacitance due to very small area of the collecting column, which can improve the detector energy resolution; and (6) natural isolation of pixels from each other due to the trench walls, which will again improve the detector energy resolution.

More details in detector CCE simulations and more 3D simulation results on other geometries (e.g. hexangular) and types will be published soon elsewhere due to space limitation here. BNL 3D-Trench electro detectors with materials other than Si; other configurations (such as SOI and supporting wafer) for fully penetrating trenches and or columns, etc. are fully described in the PCT patent application [12,13], and may be published later. The mask set of the first prototype production of the BNL 3D-Trench-Electrode Si detectors, also with some edgeless detectors, has been designed and made. The production of the first prototype has begun at CNM in Spain since January 2011 with first batch of BNL 3D-Trench-Electrode Si detectors ready for testing in September 2011.

Acknowledgments

The author would like to thank Dr. V. Radeka and Dr. D. Lynn of BNL, J. Harkonen of HIP, and V. Eremin of PTI for helpful discussions related to this work. This work was supported by the US Department of Energy, Contract no. DE-AC02-98CH10886.

References

[1] S. Parker, C. Kenney, J. Segal, Nucl. Instr. and Meth. A395 (1997) 328.
[2] C.J. Kenney, S.I. Parker, J. Segal, C. Storment, IEEE Trans. Nucl. Sci. NS46 (4) (1999) 1224.
[3] Zheng Li, M. Abreu, P. Anbinderis, et al., Nucl. Instr. and Meth. A572 (2007) 305.
[4] C. Piemonte, M. Boscardin, G.F. Dalla Betta, S. Ronchin, N. Zorzi, Nucl. Instr. and Meth. A541 (2005) 441.
[5] Z. Li, W. Chen, Y.H. Guo, D. Lissauer, D. Lynn, V. Radeka, G. Pellegrini, Nucl. Instr. and Meth. A 583 (2007) 139.
[6] Tanja Grönlund, Zheng Li, Gabriella Carini, Michael Li, Nucl. Instr. and Meth. A 586 (2008) 180.
[7] J. Kalliopuska, S. Eranen, Nucl. Instr. and Meth. A568 (2006) 22.
[8] A. Zoboli, et al., IEEE TNS 55-5 (2008) 2775.
[9] G. Pellegrini, M. Lozano, M. Ullán, R. Bates, C. Fleta, D. Pennicard, Nucl. Instr. and Meth. A 592 (2008) 38.
[10] G.-F. Dalla Betta, et al., Development of modified 3D detectors at FBK in 2010, IEEE Nuclear Science Symposium, Knoxville, TN, USA, October 30–November 6, 2010, paper N15–3.
[11] C. Kenney, et al., IEEE TNS, Trans. Nucl. Sci. NS48 (6) (2001) 2405.
[12] US Patent application, 3D Trench Electrode Detectors, filed by BNL/BSA on 10/29/2009, 1004305-027US (61/525,756).
[13] US Patent Application Converted into International Patent Application, 3D Trench Electrode Detectors, by BNL/BSA on 10/17/2010 (PCT/US2010/52887).
[14] Z. Li, New detectors with novel electrode configurations for applications in sLHC and photon sciences, presented at the Fifteenth Workshop of CERN RD50, CERN, Geneva, Switzerland, 16–18 November, 2009, 〈http://indico.cern.ch/getFile.py/access?contribId=8&sessionId=8&resId=0&materialId=slides&confId=65918〉.
[15] B. Dezillie, Z. Li, V. Eremin, W. Chen, L.J. Zhao, IEEE Trans. Nucl. Sci. NS47 (6) (2000) 1892.
[16] V. Radeka, Ann. Rev. Nucl. Part. Sci. 38 (1988) 217.
[17] Z. Li, H.W. Kraner, Nucl. Phys. B 32 (1993) 398.
[18] H. Kraner, et al., Nucl. Instr. and Meth. A326 (1993) 398.
[19] G. Kramberger, presented at CERN RD48 Workshop, Geneva, March, 2000.
[20] A. Chilingarov, presented at CERN RD48 Workshop, Geneva, March, 2000.
[21] T.J. Brodbeck, et al., Nucl. Instr. and Meth A455 (2000) 645.
[22] G. Kramberger, et al., Nucl. Instr. and Meth. A76 (2002) 645.